scientific reports

Check for updates

OPEN

Exploring soliton solutions and dynamical features of three dimensional Gardner Kadomtsov Petviashvili equation

Amjad Hussain[1]✉, Muhammad Zeeshan[1], Muhammad Junaid U Rehman[2] & Adil Jhangeer[3,4]

In this paper, the dynamical features and soliton structures of the Gardner-Kadomtsov-Petviashvili equation in three dimensions are looked at. The Jacobi elliptic function method yields wave solutions that display distinct behaviors based on parameter variations. We reformulate the system into a planar dynamical system via the Galilean transformation for further analysis.Phase portraits are depicted by adjusting the bifurcation parameters , while periodic and super nonlinear periodic wave solutions are portrayed using numerical simulations. Furthermore, quasi-periodic and chaotic behavior is depicted by varying the external forcing term and using tools such as Lyapunov exponents, Poincaré maps, and sensitivity analysis. Changes in frequency and amplitude strongly influence the system's dynamics, offering insights that can improve predictions, enhance control methods, and optimize model performance.

Keywords (3+1)-dimensional Gardner–Kadomtsov–Petviashvili equation, Soliton solutions, Jacobi elliptic function method, Phase portraits, Quasi-periodic and chaotic behavior

The investigation of the dynamical features of partial differential equations (PDEs) via different dynamics tools, such as bifurcation theory and sensitivity analysis, is ongoing. Such investigations play a prime role in the study of complex phenomena in optical systems, quantum physics, and fluid dynamics. Although considerable progress has been achieved, chaos in complex systems is still far from fully comprehended by any researcher[1]. The detection of chaos in nonlinear systems requires appropriate analytical techniques with phase portraits, bifurcation diagrams, power spectrum analysis, nonlinear time series analysis, Poincaré maps, and Lyapunov exponents, some of which may provide appropriate insight into the particular situation of the systems under study. Due to this complexity, a strong analysis will often adopt multiple methodologies, ensuring an in-depth understanding of this system[2,3]. Recently, several dynamic properties of different PDEs have attracted much attention because most of these equations admit localized solutions called solitons, among other forms of traveling waves. In this respect, the analysis of bifurcation and chaos theory is complementary, since the former investigates how changes in parameters affect stability and spatial patterns, while the latter points out the thresholds beyond which instability and chaotic behavior arise[4,5]. Together, these methods shed light on the interplay between stability and chaos[6–8], which is important to understand the underlying dynamics of nonlinear systems. Moreover, related non-linear equations are often studied using bifurcation analysis and chaos detection methods[17–19]. For example, the bifurcation and chaotic behaviors of the KdV-MKdV equations[9] have been studied in detail and provide important information about complex wave phenomena. However, the study of soliton solutions to non-linear systems is equally important, as it has many applications in science and engineering. Soliton solutions help us to understand the complex behavior of nonlinear systems. The significance of soliton solutions in several physical contexts, such as wave propagation and optical systems, has been highlighted in earlier research[10–14].

The Gardner equation models internal waves in stratified fluids and has applications in plasma physics[15] and Bose-Einstein condensates[16]. The multi-dimensional Gardner-KP equation is vital in ocean engineering, describing nonlinear internal waves on ocean shelves. Studies have shown its role in governing dispersive surface

[1]Department of Mathematics, Quaid-i-Azam University, 45320, Islamabad 44000, Pakistan. [2]Department of Automation, Biomechanics, and Mechatronics, Lodz University of Technology, 1/15 Stefanowski st., 90- 537, Łódź, Poland. [3]IT4Innovations, VSB-Technical University of Ostrava, Ostrava-Poruba, Czech Republic. [4]Center for Theoretical Physics, Khazar University, 41 Mehseti Str., Baku AZ1096, Azerbaijan. ✉email: a.hussain@qau.edu.pk

waves near critical depths[20], dispersive shock waves through the cylindrical Gardner equation[21], and solitary wave solutions[22]. In addition, elliptic and traveling wave solutions[23] and solitons have been developed using the Hirota bilinear method[24]. The (3 + 1)-dimensional Gardner-KP equation is an extended form of the (2 + 1)-dimensional Gardner-KP equation[25,26], which serves as the primary focus of this study.

The (3+1)-dimensional nonlinear Gardner–Kadomtsov–Petviashvili (Gardner-KP) equation, a notable nonlinear partial differential equation, serves as an important model for examining soliton dynamics and chaotic phenomena:

$$\left(\Psi_\sigma + 6\Psi\Psi_\phi - 6\Psi^2\Psi_\phi + \nu^2\Psi_{\phi\phi\phi}\right)_\phi + \mu\left(\Psi_{\beta\beta} + \Psi_{\xi\xi}\right) = 0, \tag{1}$$

where $\mu = \pm 1$ and $\Psi = \Psi(\phi, \beta, \xi, \sigma)$ is the real field representing the amplitude of the wave, σ is the temporal component, and ϕ, β, ξ are the spatial components.

Equation (1) models the evolution of the nonlinear wave amplitude $\Psi(\phi, \beta, \xi, \sigma)$ in a multidimensional medium. The terms appearing in (1) have the following physical meanings:

- Ψ_σ: temporal change of the wave amplitude.
- $6\Psi\Psi_\phi$: quadratic nonlinearity representing wave steepening effects.
- $-6\Psi^2\Psi_\phi$: cubic nonlinearity accounting for higher-order nonlinear interactions.
- The term $\nu^2\Psi_{\phi\phi\phi}$ is used for dispersive behavior caused by waves spreading and dispersing in the ϕ direction and ν^2 controls how much dispersion there is.
- $\mu(\Psi_{\beta\beta} + \Psi_{\xi\xi})$, that describes wave modulation in β and ξ directions and $\mu = \pm 1$ shows if this is dispersion or anti-dispersion.

Despite the numerous existing works on lower-dimensional Gardner-KP equations, they seem to lack comprehensive coverage of the (3+1)-dimensional case, particularly in terms of its explicit soliton solutions and intricate soliton dynamics. It is complicated to study the influence of various features in systems that are nonlinear, and such analysis usually requires sophisticated methods to show chaos and supernonlinear waves. We address these gaps by employing the Jacobi elliptic function method to derive new exact solutions and by investigating various aspects of the nonlinear model, as it is significant for ocean engineering, plasma physics, and wave studies.

Consequently, this paper aims to derive soliton solutions by the JEF technique[27] and to analyze the dynamics[28] of the (3 + 1)-dimensional Gardner-KP equation. This research is centred on achieving two key objectives The first one is to derive exact soliton solutions of the (3+1)-dimensional nonlinear Gardner–Kadomtsov–Petviashvili (Gardner-KP) equation using the efficient JEF technique, and the second is to investigate its nonlinear dynamics through advanced analytical tools, including chaos detection methods, Lyapunov exponents, Poincaré maps, sensitivity analysis, and phase plane analysis. These methods offer a systematic framework for investigating the equation's shift from regular behavior to chaotic dynamics.

By using a thorough methodology to reveal the soliton dynamics and nonlinear features of the (3+1)-dimensional nonlinear Gardner–Kadomtsov–Petviashvili (Gardner-KP), this study expands and improves upon previous research. By examining the chaotic and bifurcation aspects of the system, this work fills in knowledge gaps in the study of solitons and opens the door to more extensive applications in science and engineering.

Findings from this problem are very different from results obtained in earlier studies based on lower-dimensional Gardner-KP equations[24]. Unlike previous works, we highlight new and complex dynamical behaviors and additional, richer soliton structures of the (3+1)-dimensional model. The soliton solutions found using the Jacobi elliptic function method reveal new ways that pulses can interact and take shape, which are more advanced than what was seen in traditional results. Stability tests show that the results remain reliable even when changing parameters, and further analysis using phase portraits and Lyapunov exponents reveals complex stability patterns, different levels of chaos and additional features not seen in lower dimensions. This comparison shows how significant the effects of multidimensional nonlinear wave propagation are and highlights the main Gardner-KP equations used in this research, which help both the theory and practical applications.

The structure of this paper is as follows: The first part uses the Jacobi elliptic method to find the soliton solutions of the (3+1)-dimensional Gardner-KP equation. In the second part, the dynamic behaviour of the same model is analyzed using various tools, such as phase portraits, bifurcation analysis, and Lyapunov exponents, to investigate its chaotic and quasiperiodic dynamics.

Soliton Solution of the (3 + 1)-dimensional Gardner-KP equation by JEF Technique

Jacobi elliptic functions, first described by Carl Gustav Jacob Jacobi in 1827, are periodic functions derived as the inverses of elliptic integrals. They are essential in areas such as mathematical physics, nonlinear dynamics and differential equations. The main Jacobi elliptic functions are $\mathrm{sn}(z|m)$, $\mathrm{cn}(z|m)$, and $\mathrm{dn}(z|m)$. They are defined in terms of a parameter *m*, which is called the elliptic modulus, and they show how the amplitude of the elliptic integral is related to its arguments. Because they are periodic and relate to each other, they are like trigonometric functions in elliptic geometry. This gives us many ways to solve hard math and science problems[29]. The detailed description of the method is provided in[27].

We use the following transformation:

$$\Psi(\phi, \beta, \xi, \sigma) = \Upsilon(\chi), \quad \text{where} \quad \chi = b_1\phi + b_2\beta + b_3\xi + c\sigma, \tag{2}$$

which defines a traveling wave solution, where

- b_1, b_2, b_3 are wave numbers corresponding to spatial directions ϕ, β, and ξ, representing the direction and wavelength of the wave.
- c is the wave speed in time, governing how fast the wave profile moves.

This transformation reduces the partial differential equation (1) to an ordinary differential equation (ODE) in χ:

$$(\mu b_3^2 + cb_1 + \mu b_2^2)\Upsilon'' + 6b_1^2(\Upsilon\Upsilon')' - 6b_1^2(2\Upsilon(\Upsilon')^2 + \Upsilon^2\Upsilon'') + \nu^2 b_1^4 \Upsilon'''' = 0, \tag{3}$$

facilitating the analysis of soliton solutions propagating in multiple spatial dimensions.

Upon the JEF method, we take the solution of Eq. (3) in the following form:

$$\Upsilon(\chi) = \sum_{l=1}^{N} k_l G^l(\chi).$$

Next, by virtue of the homogeneous balancing principle, that is balancing the highest-order derivative term with the nonlinear term, we get $N = 1$, so the solution simplifies to

$$\Upsilon(\chi) = k_0 + k_1 G(\chi), \tag{4}$$

where k_0 and k_1 are the constants and the function $G(\chi)$ satisfy the followingg ansatz

$$G'(\chi) = \sqrt{r_1 + r_2 G^2(\chi) + \frac{r_3}{2} G^4(\chi)}.$$

By substituting (4) into equation (3), we derive a system of equations. We solve this system using the computational software Maple to obtain the following parameter values.

$$\begin{cases} \mu = \mu, \quad c = c, \quad v = v, \quad k_0 = \frac{1}{2}, \quad k_1 = k_1, \quad b_1 = b_1, \quad b_2 = b_2, \quad b_3 = b_3, \\ r_1 = r_1, \quad r_2 = -\frac{1}{2} \times \frac{2\mu b_2^2 + 2\mu b_3^2 + 3b_1^2 + 2(c \cdot b_1)}{v^2 b_1^2}, \\ r_3 = \frac{2k_1^2}{v^2}. \end{cases} \tag{5}$$

Family 1: When the parameters are defined as $r_1 = 1$, $r_2 = -(1 + \delta^2)$, and $r_3 = 2\delta^2$, the wave profile can be derived from analyzing $G(\chi)$, where the function is expressed using the Jacobi elliptic sine function, $\mathrm{sn}(\chi, \delta)$:

$$\Upsilon(\chi) = k_0 + k_1 \,\mathrm{sn}(\chi, \delta).$$

Specifically, in this case, the wave profile simplifies to

$$\Upsilon(\chi) = \frac{1}{2} + k_1 \,\mathrm{sn}(\chi, \delta).$$

As the parameter δ approaches 1, the shock wave profile transitions into the following form, represented using the hyperbolic tangent function:

$$\Upsilon(\chi) = \frac{1}{2} + k_1 \tanh(\chi).$$

To further generalize this result, we can express the shock wave profile as follows:

$$\Psi(\phi, \beta, \xi, \sigma) = \frac{1}{2} + k_1 \tanh(b_1\phi + b_2\beta + b_3\xi + c\sigma). \tag{6}$$

Family 2: Consider the parameters $r_1 = -\delta^2(1 - \delta^2)$, $r_2 = 2\delta^2 - 1$, and $r_3 = 2$. By choosing $G(\chi) = \mathrm{ds}(\chi, \delta)$, we derive a periodic wave profile given by:

$$\Upsilon(\chi) = \frac{1}{2} + k_1 \,\mathrm{ds}(\chi, \delta).$$

When the parameter δ approaches 1, the wave profile transitions into the following form involving the hyperbolic cosecant function:

$$\Upsilon(\chi) = \frac{1}{2} + k_1 \,\mathrm{csch}(\chi).$$

This result can be further generalized for a multidimensional scenario, where the wave profile is expressed as:

$$\Psi(\phi, \beta, \xi, \sigma) = \frac{1}{2} + k_1 \,\mathrm{csch}(b_1\phi + b_2\beta + b_3\xi + c\sigma).$$

Family 3: When the parameters are defined as $r_1 = 1 - \delta^2$, $r_2 = 2 - \delta^2$, and $r_3 = 2$, the periodic wave profile can be derived by analyzing $G(\chi) = \mathrm{cs}(\chi, \delta)$. This leads to the expression:

$$\Upsilon(\chi) = \frac{1}{2} + k_1 \,\mathrm{cs}(\chi, \delta).$$

As the parameter δ approaches the limiting case of $\delta \to 1$, the profile transforms into:

$$\Upsilon(\chi) = \frac{1}{2} + k_1 \coth(\chi).$$

Extending this into a multidimensional framework, the wave profile is given by:

$$\Psi(\phi, \beta, \xi, \sigma) = \frac{1}{2} + k_1 \coth(b_1\phi + b_2\beta + b_3\xi + c\sigma).$$

Family 4: For the parameters $r_1 = 1 - \delta^2$, $r_2 = 2\delta^2 - 1$, and $r_3 = -2\delta^2$, the periodic wave structure can be described by analyzing $G(\chi) = \mathrm{cn}(\chi, \delta)$ The resulting wave form is:

$$\Upsilon(\chi) = \frac{1}{2} + k_1 \,\mathrm{cn}(\chi, \delta).$$

In the special case where $\delta \to 1$, the wave profile transitions to the following form involving the hyperbolic secant function:

$$\Upsilon(\chi) = \frac{1}{2} + k_1 \,\mathrm{sech}(\chi).$$

Moreover, the generalized multidimensional form of the wave profile is expressed as:

$$\Psi(\phi, \beta, \xi, \sigma) = \frac{1}{2} + k_1 \,\mathrm{sech}(b_1\phi + b_2\beta + b_3\xi + c\sigma). \tag{7}$$

Family 5: For the parameters $r_1 = \delta^2 - 1$, $r_2 = 2 - \delta^2$, and $r_3 = -2$, the periodic wave profile can be determined by analyzing $G(\chi) = \mathrm{dn}(\chi, \delta)$. The expression for the wave profile is given by:

$$\Upsilon(\chi) = \frac{1}{2} + k_1 \,\mathrm{dn}(\chi, \delta).$$

In the limiting case as $\delta \to 1$, the wave profile simplifies to the hyperbolic secant form:

$$\Upsilon(\chi) = \frac{1}{2} + k_1 \,\mathrm{sech}(\chi).$$

Furthermore, the wave profile can be extended into a multidimensional representation as follows:

$$\Psi(\phi, \beta, \xi, \sigma) = \frac{1}{2} + k_1 \,\mathrm{sech}(b_1\phi + b_2\beta + b_3\xi + c\sigma).$$

Family 6: For the parameters $r_1 = \frac{1}{4}$, $r_2 = \frac{\delta^2 - 2}{2}$, and $r_3 = \frac{\delta^2}{2}$, the double-periodic wave structure is described by analyzing $G(\chi) = \frac{\mathrm{sn}(\chi, \delta)}{1 \pm \mathrm{dn}(\chi, \delta)}$. The resulting wave form is:

$$\Upsilon(\chi) = \frac{1}{2} + \frac{k_1 \,\mathrm{sn}(\chi, \delta)}{1 \pm \mathrm{dn}(\chi, \delta)}.$$

In the special case where $\delta \to 1$, the wave profile becomes:

$$\Psi(\phi, \beta, \xi, \sigma) = \frac{1}{2} + \frac{k_1 \tanh(\ b_1\phi + b_2\beta + b_3\xi + c\sigma)}{1 \pm \mathrm{sech}(b_1\phi + b_2\beta + b_3\xi + c\sigma)}. \tag{8}$$

Family 7: For the parameters $r_1 = \frac{\delta^2}{4}$, $r_2 = \frac{\delta^2 - 2}{2}$, and $r_3 = \frac{\delta^2}{2}$, the double-periodic wave structure is described by analyzing $G(\chi) = \frac{\mathrm{sn}(\chi, \delta)}{1 \pm \mathrm{dn}(\chi, \delta)}$. The resulting wave form is:

$$\Upsilon(\chi) = \frac{1}{2} + \frac{k_1 \,\mathrm{sn}(\chi, \delta)}{(\delta^2 + 1)(\mathrm{sn}(\chi, \delta) 1 \pm \mathrm{dn}(\chi, \delta))}.$$

In the special case where $\delta \to 1$, the wave profile transitions to:

$$\Upsilon(\chi) = \frac{1}{2} + \frac{k_1 \tanh(\chi)}{1 \pm \operatorname{sech}(\chi)}.$$

$$\Psi(\phi, \beta, \xi, \sigma) = \frac{1}{2} + \frac{k_1 \tanh(\ b_1\phi + b_2\beta + b_3\xi + c\sigma)}{1 \pm \operatorname{sech}(\ b_1\phi + b_2\beta + b_3\xi + c\sigma)}.$$

Family 8: For the parameters $r_1 = -\frac{(1-\delta^2)^2}{4}$, $r_2 = \frac{\delta^2+1}{2}$, and $r_3 = -\frac{1}{2}$, the double-periodic wave structure is described by analyzing $G(\chi) = \operatorname{cn}(\chi, \delta) \pm \operatorname{dn}(\chi, \delta)$. The resulting wave form is:

$$\Upsilon(\chi) = \frac{1}{2} + k_1(\operatorname{cn}(\chi, \delta) \pm \operatorname{dn}(\chi, \delta)).$$

In the special case where $\delta \to 1$, the wave profile becomes:

$$\Upsilon(\chi) = \frac{1}{2} + k_1(\operatorname{sech}(\chi) \pm \operatorname{sech}(\chi)).$$

$$\Psi(\phi, \beta, \xi, \sigma) = \frac{1}{2} + k_1(\operatorname{sech}(b_1\phi + b_2\beta + b_3\xi + c\sigma) \pm \operatorname{sech}(\ b_1\phi + b_2\beta + b_3\xi + c\sigma)).$$

Family 9: For the parameters $r_1 = \frac{\delta^2-1}{4}$, $r_2 = \frac{\delta^2+1}{2}$, and $r_3 = \frac{\delta^2-1}{2}$, the double-periodic wave structure is described by analyzing $G(\chi) = \frac{\operatorname{dn}(\chi,\delta)}{1 \pm \operatorname{sn}(\chi,\delta)}$. The resulting wave form is:

$$\Upsilon(\chi) = \frac{1}{2} + \frac{k_1 \operatorname{dn}(\chi, \delta)}{1 \pm \operatorname{sn}(\chi, \delta)}.$$

In the special case where $\delta \to 1$, the wave profile transitions to:

$$\Upsilon(\chi) = \frac{1}{2} + \frac{k_1 \operatorname{sech}(\chi)}{1 \pm \tanh(\chi)}.$$

$$\Psi(\phi, \beta, \xi, \sigma) = \frac{1}{2} + \frac{k_1 \operatorname{sech}(\ b_1\phi + b_2\beta + b_3\xi + c\sigma)}{1 \pm \tanh(\ b_1\phi + b_2\beta + b_3\xi + c\sigma)}.$$

Family 10: For the parameters $r_1 = \frac{1-\delta^2}{4}$, $r_2 = \frac{1-\delta^2}{2}$, and $r_3 = \frac{1-\delta^2}{2}$, the double-periodic wave structure is described by analyzing $G(\chi) = \frac{\operatorname{cn}(\chi,\delta)}{1 \pm \operatorname{sn}(\chi,\delta)}$. The resulting wave form is:

$$\Upsilon(\chi) = \frac{1}{2} + \frac{k_1 \operatorname{cn}(\chi, \delta)}{1 \pm \operatorname{sn}(\chi, \delta)}.$$

In the special case where $\delta \to 1$, the wave profile transitions to:

$$\Upsilon(\chi) = \frac{1}{2} + \frac{k_1 \operatorname{sech}(\chi)}{1 \pm \tanh(\chi)}.$$

$$\Psi(\phi, \beta, \xi, \sigma) = \frac{1}{2} + \frac{k_1 \operatorname{sech}(\ b_1\phi + b_2\beta + b_3\xi + c\sigma)}{1 \pm \tanh(\ b_1\phi + b_2\beta + b_3\xi + c\sigma)}.$$

Family 11: For the parameters $r_1 = \frac{1}{4}$, $r_2 = \frac{(1-\delta^2)^2}{2}$, and $r_3 = \frac{(1-\delta^2)^2}{2}$, the double-periodic wave structure is described by analyzing $G(\chi) = \frac{\operatorname{sn}(\chi,\delta)}{\operatorname{dn}(\chi,\delta) \pm \operatorname{cn}(\chi,\delta)}$. The resulting wave form is:

$$\Upsilon(\phi, \beta, \xi, \sigma) = \frac{1}{2} + \frac{k_1 \operatorname{sn}(\chi, \delta)}{\operatorname{dn}(\chi, \delta) \pm \operatorname{cn}(\chi, \delta)}.$$

In the special case where $\delta \to 1$, the wave profile becomes:

$$\Upsilon(\chi) = \frac{1}{2} + \frac{k_1 \tanh(\chi)}{\operatorname{sech}(\chi) \pm \operatorname{sech}(\chi)}.$$

$$\Psi(\phi, \beta, \xi, \sigma) = \frac{1}{2} + \frac{k_1 \tanh(\ b_1\phi + b_2\beta + b_3\xi + c\sigma)}{\operatorname{sech}(\ b_1\phi + b_2\beta + b_3\xi + c\sigma) \pm \operatorname{sech}(\ b_1\phi + b_2\beta + b_3\xi + c\sigma)}. \tag{9}$$

Family 12: For the parameters $r_1 = 0$, $r_2 = 0$, and $r_3 = 2$, the rational structure is described by analyzing $G(\chi) = \frac{D}{\chi}$. The resulting wave form is:

$$\Upsilon(\chi) = \frac{1}{2} + \frac{k_1 D}{\chi}.$$

In the special case where $\delta \to 1$, the expression remains:

$$\Psi(\phi, \beta, \xi, \sigma) = \frac{1}{2} + \frac{k_1 D}{(\, b_1\phi + b_2\beta + b_3\xi + c\sigma)}.$$

Family 13: For the parameters $r_1 = 0$, $r_2 = 1$, and $r_3 = 0$, the rational structure is described by analyzing $G(\chi) = \frac{1}{2} + De^{\chi}$. The resulting wave form is:

$$\Upsilon(\chi) = \frac{1}{2} + b_1 De^{\chi}.$$

In the special case where $\delta \to 1$, the expression remains:

$$\Psi(\phi, \beta, \xi, \sigma) = \frac{1}{2} + b_1 De^{(\, b_1\phi + b_2\beta + b_3\xi + c\sigma)}.$$

Analyzing physical dynamics through visualization

We employ visual representations for the novel soliton structures of the non-linear Gardner-KP equation . These pictures show the newly calculated waveform solutions in the form of graphs. The solutions include hyperbolic, trigonometric, and rational forms from different Familys. The physical interpretation of these solutions is facilitated by simulations conducted using the symbolic computation software Mathematica. Soliton structures that can be recognized include double periodic waves, shock wave solutions, kink-shaped solitons, solitary or bell-shaped solitons, and periodic wave soliton solutions. Each has its set of physical properties. The shock wave soliton solution is shown in Fig. 1, the bell-shaped soliton solution is shown in Fig. 2, and the kink type, which shows the smooth transition of soliton solutions, is shown in Figs. 3 and 4.

To provide physical insight, these various soliton solutions correspond to real nonlinear wave phe-nomena observed in fluids and plasma. For example, shock wave solutions model abrupt changes in wave amplitude analogous to physical shock fronts, while bell-shaped solitary waves represent stable waves as they can propagate without distortion and are localized. Kink solitons describe smooth transitions with changing state of waves and are akin to stable domains found in many media. Thus, these solutions outline both valuable mathematical patterns and important meanings related to oceanography, plasma physics and nonlinear wave propagation.

Shock wave profile

We evaluate the features of the shock wave solutions described by equation (6). As seen in Fig. 1, the wave is shaped in a certain manner for these selected parameter values. The extreme change in the gradient illustrates the common nonlinear steepening seen in shock effects that happen in fluids and plasmas.

Bell-shaped soliton

The wave solution in the form of a bell-shaped soliton appears in Fig. 2. Such a profile remains fixed in shape as it travels, which is common with nonlinear waves, like internal waves found in fluids.

Kink-type soliton

Smooth changes from one wave state to another are seen in Figs. 3 and 4 from the kink-type soliton solutions. They show how stable wave motions, like a front, frequently appear in various physical situations.

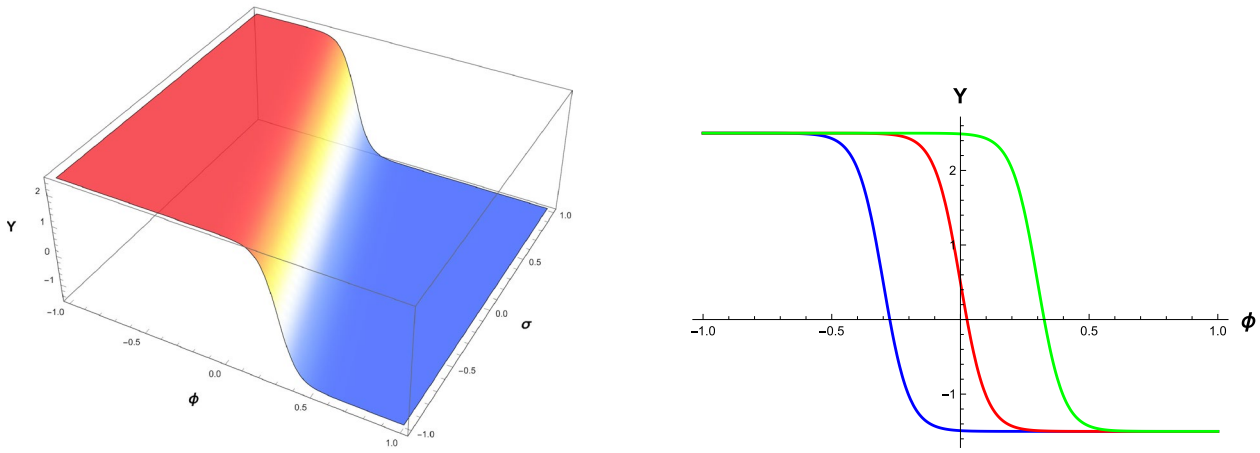

(a) 3D Wave Profile. (b) 2D Wave Profile.

Fig. 1. Wave Profile Visualization of the equation (6) with parameters $k_1 = 2$, $b_1 = 10$, $b_2 = 5$, $b_3 = -10$, and $c = 3$.Figures generated using Mathematica Version 13.3.1.0 (Wolfram Research, Champaign, IL, USA; https://www.wolfram.com/mathematica/).

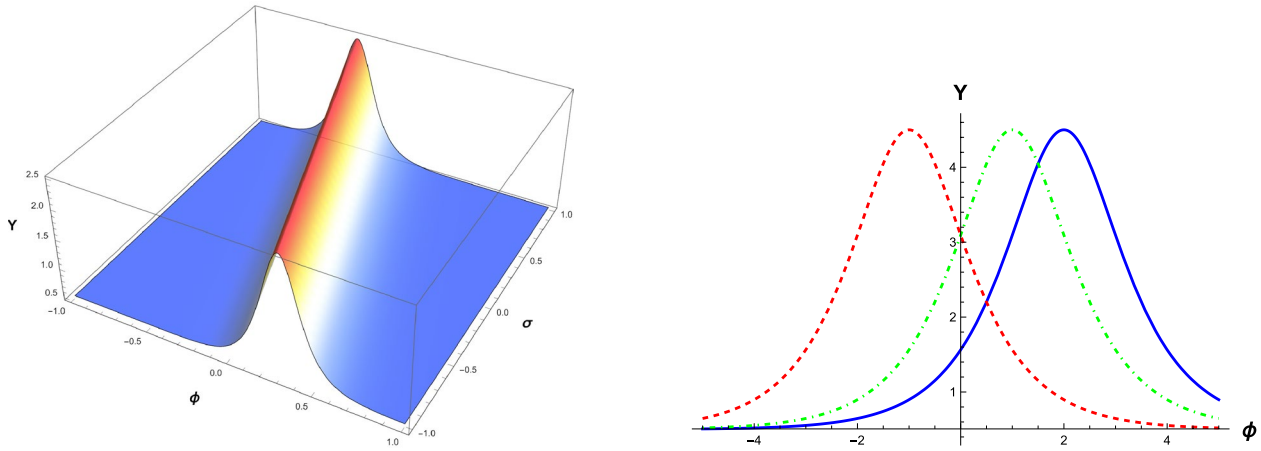

(a) 3D wave profile. (b) 2D wave profile.

Fig. 2. Wave Profile Visualization of equation (7) with parameters $k_1 = 2$, $b_1 = 10$, $b_2 = 5$, $b_3 = -10$, and $c = 3$.Figures generated using Mathematica Version 13.3.1.0 (Wolfram Research, Champaign, IL, USA; https://www.wolfram.com/mathematica/).

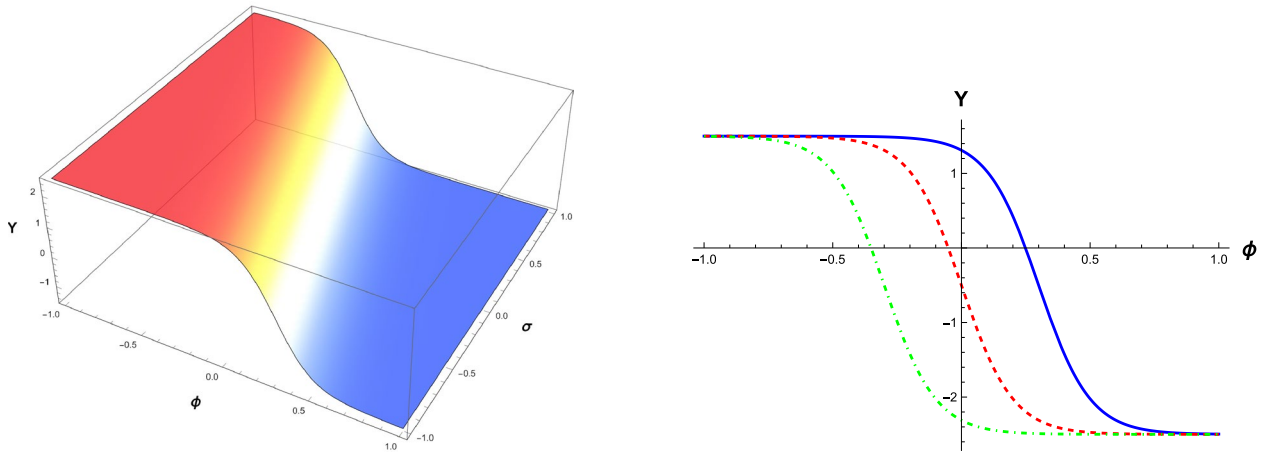

(a) 3D wave profile. (b) 2D wave profile.

Fig. 3. Wave Profile Visualization of equation (8) with parameters $k_1 = 2$, $b_1 = 10$, $b_2 = 5$, $b_3 = -10$, and $c = 3$.Figures generated using Mathematica Version 13.3.1.0 (Wolfram Research, Champaign, IL, USA; https://www.wolfram.com/mathematica/).

Numerical stability analysis of the obtained soliton solutions

For stability, a small amplitude-scaled Gaussian perturbation is added to the above-plotted soliton profile, and these perturbations are observed over time. The perturbation magnitude was evaluated by calculating the norm of the difference between the perturbed and original soliton solutions at various time instances. Every soliton solution showed a decrease in perturbation norm, as the table presented in Table 1 shows, indicating that each soliton is locally stable to small perturbations. Hence, it can be said that solitons are stable when focused on their immediate surrounding points in the solution space[30,31].

The local stability means that soliton solutions are being considered very close to their exact values. It does not rule out that other types of dynamics and even chaotic dynamics can develop at the larger scales discussed further in the dynamical section.

Dynamical analysis of Gardner-Kp equation

Studying the dynamics of the (3+1)-dimensional Gardner-KP equation helps explain the stability of solitons in real situations. Phase portraits, Lyapunov exponents, and Poincaré maps explain how the waves behave, staying the same or sometimes changing to chaos or complex patterns. Seeing these dynamics clearly helps explain how

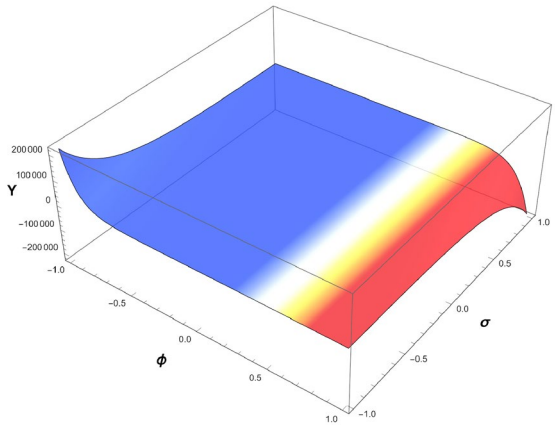

(a) 3D wave profile.

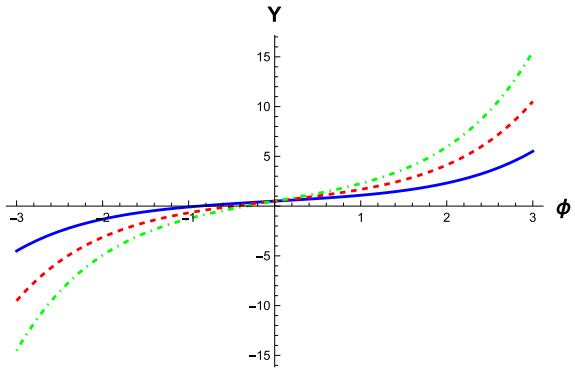

(b) 2D wave profile.

Fig. 4. Wave Profile Visualization of equation (9) with parameters $k_1 = 2$, $b_1 = 10$, $b_2 = 5$, $b_3 = -10$, and $c = 3$.Figures generated using Mathematica Version 13.3.1.0 (Wolfram Research, Champaign, IL, USA; https://www.wolfram.com/mathematica/).

Time t	$\|\Delta U_1\|_2$	$\|\Delta U_2\|_2$	$\|\Delta U_3\|_2$	$\|\Delta U_4\|_2$
0.00	0.495	0.561	0.384	2.699
1.01	0.299	0.339	0.232	1.629
2.02	0.180	0.204	0.140	0.983
3.03	0.109	0.123	0.084	0.593
4.04	0.066	0.074	0.051	0.358
5.05	0.040	0.045	0.031	0.216
6.06	0.024	0.027	0.019	0.130
7.07	0.014	0.016	0.011	0.079
8.08	0.009	0.010	0.007	0.047
9.09	0.005	0.006	0.004	0.029

Table 1. Perturbation norms $\|\Delta U_i\|_2$ of the plotted soliton solutions at selected times.

nonlinear waves change, connect, and travel in materials such as fluids and plasma. For such an analysis, we integrate Equation (3) twice to get

$$\Upsilon'' - \frac{2}{\nu^2 b_1^2}\Upsilon^3 + \frac{3}{\nu^2 b_1^2}\Upsilon^2 + \frac{\mu b_3^2 + c b_1 + \mu b_2^2}{\nu^2 b_1^4}\Upsilon = 0.$$

Letting $\alpha_1 = \frac{2}{\nu^2 b_1^2}$, $\alpha_2 = \frac{3}{\nu^2 b_1^2}$ and $\alpha_3 = \frac{\mu b_3^2 + c b_1 + \mu b_2^2}{\nu^2 b_1^4}$ we obtain

$$\Upsilon'' - \alpha_1 \Upsilon^3 + \alpha_2 \Upsilon^2 + \alpha_3 \Upsilon = 0.$$

Finally, we apply the Galilean transformation to get

$$\Upsilon' = \Gamma, \quad \Gamma' = \alpha_1 \Upsilon^3 - \alpha_2 \Upsilon^2 - \alpha_3 \Upsilon, \tag{10}$$

The equilibrium points of (10) are determined by letting

$$\Upsilon' = 0 \quad \text{and} \quad \Gamma' = 0.$$

These conditions, when substituted in (10) yield:

$$\Gamma = 0 \quad \text{and} \quad \alpha_1 \Upsilon^3 - \alpha_2 \Upsilon^2 - \alpha_3 \Upsilon = 0,$$

which on solving, results in

$$\Gamma = 0 \quad \text{and} \quad \Upsilon = 0, \quad \frac{\alpha_2 \pm \sqrt{\alpha_2^2 + 4\alpha_1\alpha_3}}{2\alpha_1}.$$

The system has three equilibrium points: $E_0(\Upsilon_0, 0)$, $E_1(\Upsilon_1, 0)$, and $E_2(\Upsilon_2, 0)$, where

$$\Upsilon_0 = 0, \quad \Upsilon_1 = \frac{\alpha_2 + \sqrt{\alpha_2^2 + 4\alpha_1\alpha_3}}{2\alpha_1}, \quad \Upsilon_2 = \frac{\alpha_2 - \sqrt{\alpha_2^2 + 4\alpha_1\alpha_3}}{2\alpha_1}.$$

The Jacobian matrix for the system (10) can be expressed as

$$J_m(\Upsilon_i, \Gamma_i) = \begin{pmatrix} 0 & 1 \\ 3\alpha_1\Upsilon_i^2 - 2\alpha_2\Upsilon_i - \alpha_3 & 0 \end{pmatrix}, \ i = 0, 1, 2.$$

Let $M(\Upsilon_i, 0)$ be the coefficient matrix of the linearized system at the equilibrium point $(\Upsilon_i, 0)$:

$$M(\Upsilon_i, 0) = \begin{pmatrix} 0 & 1 \\ 3\alpha_1\Upsilon_i^2 - 2\alpha_2\Upsilon_i - \alpha_3 & 0 \end{pmatrix}.$$

At the equilibrium point $(\Upsilon_i, 0)$, we define the determinant J and trace T of matrix M. The determinant J is given by:

$$J = \alpha_3 + 2\alpha_2\Upsilon - 3\alpha_1\Upsilon^2,$$

and the trace $T = 0$.

The eigenvalues of the matrix M are determined by solving the characteristic equation:

$$|M - \lambda I_{2\times 2}| = 0,$$

which simplifies to

$$\lambda^2 - (3\alpha_1\Upsilon_i - 2\alpha_2\Upsilon_i - \alpha_3) = 0.$$

Thus, the eigenvalues of M are:

$$\lambda_{1,2} = \pm\sqrt{3\alpha_1\Upsilon_i^2 - 2\alpha_2\Upsilon_i - \alpha_3}.$$

These eigenvalues depend on the parameters α_1, α_2, and α_3, as well as the equilibrium points $(\Upsilon_i, 0)$. It is important to note that the parameters α_1, α_2, and α_3 are related to system parameters, such as ν, b_1, b_2, b_3, c, and μ.

The stability of the critical points $(\Upsilon_i, 0)$ can be analyzed based on Table 2.

As the system (10) is a three-parameter planar dynamical system, with the stability of the system depending on the values of parameters α_1, α_2, and α_3. The behavior of the system is further investigated by analyzing the bifurcations in the phase portraits of (10) as the parameter values change.

Phase portraits

Phase portraits are graphical representations of a dynamical system's trajectories in its phase space, showing how the system evolves over time based on initial conditions. They provide insight into the stability and behavior of equilibria, periodic orbits, and chaotic dynamics .

- **Case 1:** When α_1, α_2, and α_3 are all positive, the system has three equilibrium points: $E_0(0, 0)$ and $E_{1\pm}$. The point E_0 acts as a center, while the points E_{1-} and E_{1+} are identified as saddle points (Fig. 5-a).
- **Case 2:** In this case, α_1 is positive, α_2 is negative , α_3 is also positive. The system exhibits equilibrium points $E_0(0, 0)$ and $E_{2\pm}$. Here, E_0 is a center, while E_{2-} and E_{2+} act as saddle points. (Fig. 5-b)
- **Case 3:** If, α_1 is negative, α_2 is positive , α_3 is negative, the system has equilibrium points $E_3(0, 0)$ and $E_{3\pm}$. The equilibrium E_0 becomes a saddle point, while E_{3+} and E_{3-} are centers (Fig. 6-a).

Condition	Eigenvalue Nature	Equilibrium Type	Stability
$J < 0$	Real, opposite signs	Saddle Point	Always unstable
$J > 0, T^2 - 4J \geq 0$	Real, same sign	Node	Stable if $T < 0$, unstable if $T > 0$
$J > 0, T^2 - 4J < 0, T \neq 0$	Complex conjugates	Focus	Stable if $T < 0$, unstable if $T > 0$
$J > 0, T = 0$	Pure imaginary	Center	Neutrally stable (closed orbits)
$J = 0$, Poincaré index = 0	Degenerate	Zero Point / Cusp	Indeterminate

Table 2. Stability classification of equilibrium points based on the Jacobian matrix.

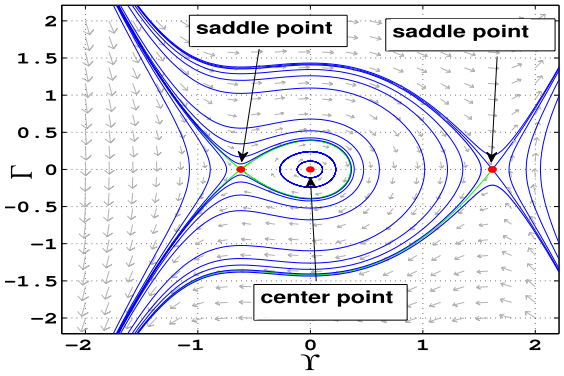

(a) Phase plot for scenario (5a).

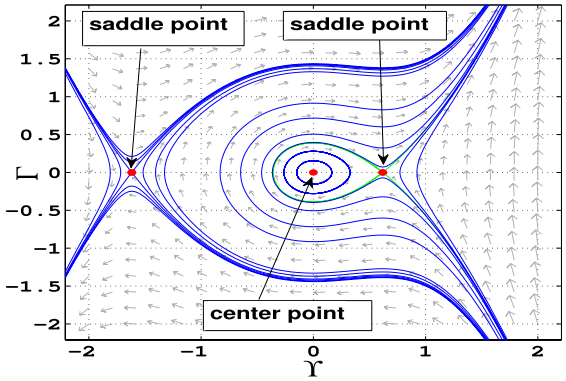

(b) Phase plot for scenario (5b).

Fig. 5. Graphical representations of the system's phase space dynamics (10).

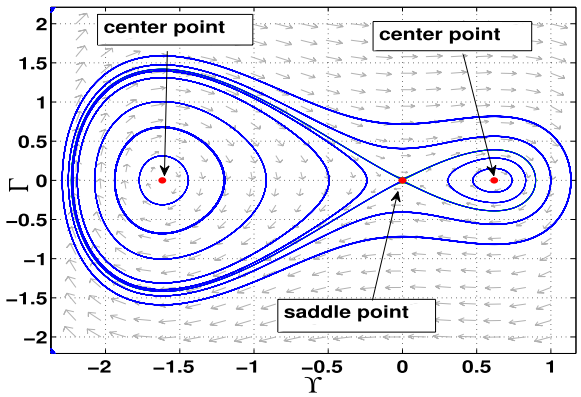

(a) Phase plot for scenario (6a).

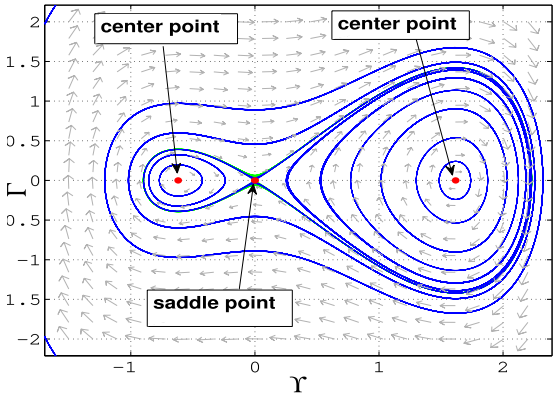

(b) Phase plot for scenario (6b).

Fig. 6. Graphical representations of the system's phase space dynamics (10).

- **Case 4:** If all parameters are negative ($\alpha_1, \alpha_2, \alpha_3 < 0$), the system contains equilibrium points $E_0(0,0)$ and $E_{4\pm}$. In this configuration, E_0 is a saddle point, while E_{4-} and E_{4+} are centers (Fig. 6-b).
- **Case 5:** If, α_1 is negative, α_2 is positive , α_3 is also Positive , only one equilibrium point: $E_0(0,0)$, which acts as a center (Fig. 7-a)
- **Case 6:** If, α_1 is negative, α_2 is negative , α_3 is also Positive , the system has only $E_0(0,0)$ as an equilibrium point. This point is identified as a center (Fig. 7-b)
- **Case 7:** If, α_1 is positive, α_2 is positive , α_3 is negative, the system has only $E_0(0,0)$ as an equilibrium point. This equilibrium point functions as a saddle (Fig. 8-a).
- **Case 8:** Finally when, α_1 is positive, α_2 is negative , α_3 is negative the system again has only $E_0(0,0)$ as an equilibrium point. Here, E_0 is classified as a saddle (Fig. 8-b).

Hamiltonian dynamics

In classical mechanics, Hamilton's equations describe systems of the form:

$$\frac{d\Upsilon}{d\chi} = U(\Upsilon, \Gamma), \quad \frac{d\Gamma}{d\chi} = V(\Upsilon, \Gamma),$$

A system is Hamiltonian if a function $H(\Upsilon, \Gamma)$ exists such that:

$$U = \frac{\partial H}{\partial \Gamma}, \quad V = -\frac{\partial H}{\partial \Upsilon}.$$

This function $H(\Upsilon, \Gamma)$ is referred to as the Hamiltonian[32].

Definition 1 A system is Hamiltonian if it satisfies:

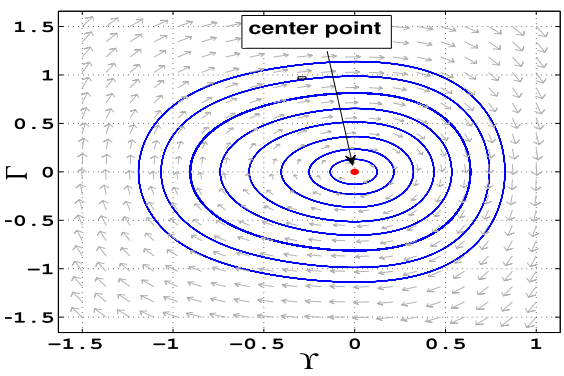

(a) Phase plot for scenario (7a).

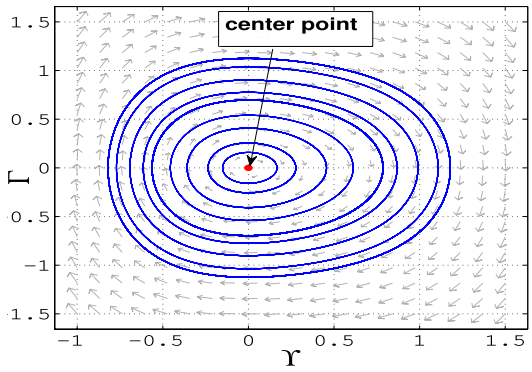

(b) Phase plot for scenario (7b).

Fig. 7. Graphical representations of the system's phase space dynamics (10).

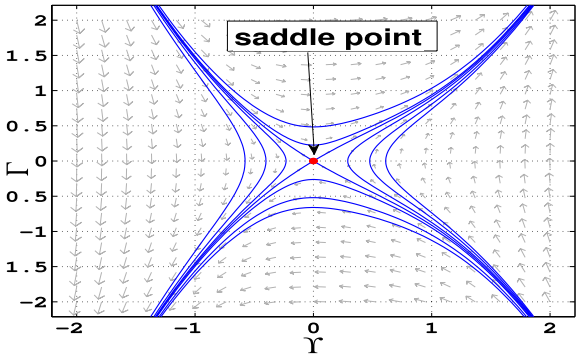

(a) Phase plot for scenario (8a).

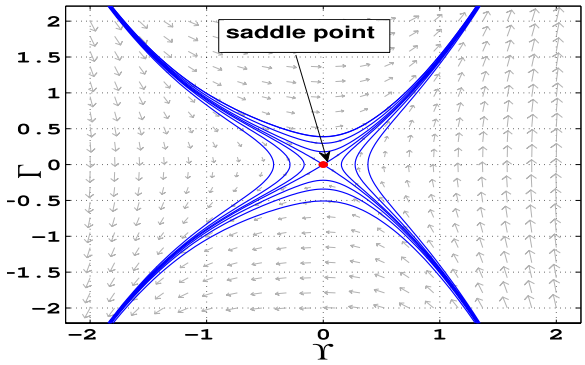

(b) Phase plot for scenario (8b).

Fig. 8. Graphical representations of the system's phase space dynamics (10).

$$\frac{\partial U}{\partial \Upsilon} + \frac{\partial V}{\partial \Gamma} = 0.$$

Equations describing the system qualify as Hamiltonian if they meet this condition:

$$\frac{\partial}{\partial \Upsilon}\left(\frac{d\Upsilon}{d\chi}\right) + \frac{\partial}{\partial \Gamma}\left(\frac{d\Gamma}{d\chi}\right) = 0.$$

The corresponding Hamiltonian function is:

$$H(\Upsilon, \Gamma) = \frac{\Gamma^2}{2} - \frac{\alpha_1}{4}\Upsilon^4 + \frac{\alpha_2}{3}\Upsilon^3 + \frac{\alpha_3}{2}\Upsilon^2.$$

Definition 2 For a critical point (Υ_0, Γ_0), the discriminant is:

$$\Omega(\Upsilon, \Gamma) = H_{\Upsilon\Upsilon} \cdot H_{\Gamma\Gamma} - (H_{\Upsilon\Gamma})^2.$$

Case 1: When the determinant $\Omega(\Upsilon_0, \Gamma_0)$ is positive, the critical point may be identified as either a local maximum or a local minimum.

Case 2: When the determinant $\Omega(\Upsilon_0, \Gamma_0)$ is negative, the critical point corresponds to a saddle point.

Case 3: If $\Omega(\Upsilon_0, \Gamma_0) = 0$, further analysis is needed.

Proposed results from Table (3) and Table (4)

Result 1: For $\alpha_1 > 0$, $\alpha_3 > 0$, and $\alpha_2^2 + 4\alpha_1\alpha_3 > 0$, the system defined by equation (10) has stable center at $(0, 0)$ and saddle points at:

For selecting α_1, α_2, and α_3	Equilibrium points	Eigenvalues	Classifications
$\alpha_1 = 1, \alpha_2 = 1, \alpha_3 = 1$ Figure 5(a)	(-0.62, 0)	±1.18	Unstable saddle
	(0, 0)	$\pm i$	Stable center
	(1.62, 0)	±1.9	Unstable saddle
$\alpha_1 = 1, \alpha_2 = -1, \alpha_3 = 1$ Figure 5(b)	(-1.62, 0)	±1.9	Unstable saddle
	(0, 0)	$\pm i$	Stable center
	(0.62, 0)	±1.18	Unstable saddle
$\alpha_1 = -1, \alpha_2 = 1, \alpha_3 = -1$ Figure 6(a)	(-1.62, 0)	±1.9i	Stable center
	(0, 0)	±1	Unstable saddle
	(0.62, 0)	±1.18i	Stable center
$\alpha_1 = -1, \alpha_2 = -1, \alpha_3 = -1$ Figure 6(b)	(-0.62, 0)	±1.18i	Stable center
	(0, 0)	±1	Unstable saddle
	(1.62, 0)	±1.9i	Stable center
$\alpha_1 = -1, \alpha_2 = 1, \alpha_3 = 1$ Figure 7(a)	(0, 0)	$\pm i$	Stable center
$\alpha_1 = -1, \alpha_2 = -1, \alpha_3 = 1$ Figure 7(b)	(0, 0)	$\pm i$	Stable center
$\alpha_1 = 1, \alpha_2 = 1, \alpha_3 = -1$ Figure 8(a)	(0, 0)	±1	Unstable saddle
$\alpha_1 = 1, \alpha_2 = -1, \alpha_3 = -1$ Figure 8(b)	(0, 0)	±1	Unstable saddle

Table 3. Phase Portraits classifications for different values of α_1, α_2, and α_3.

For selecting α_1, α_2, and α_3	Equilibrium points (Ei, 0)	Ω(Ei, 0)	Classifications
$\alpha_1 = 1, \alpha_2 = 1, \alpha_3 = 1$	(-0.62, 0)	-1.39	Saddle-node
	(0, 0)	1	Stable center
	(1.62, 0)	-3.63	Saddle-node
$\alpha_1 = 1, \alpha_2 = -1, \alpha_3 = 1$	(-1.62, 0)	-3.63	Saddle-node
	(0, 0)	1	Center-node
	(0.62, 0)	-1.39	Saddle-node
$\alpha_1 = -1, \alpha_2 = 1, \alpha_3 = -1$	(-1.62, 0)	3.63	Center-node
	(0, 0)	-1	Saddle-node
	(0.62, 0)	1.39	Center-node
$\alpha_1 = -1, \alpha_2 = -1, \alpha_3 = -1$	(-0.62, 0)	1.39	Center-node
	(0, 0)	-1	Saddle-node
	(1.62, 0)	3.63	Center-node
$\alpha_1 = -1, \alpha_2 = 1, \alpha_3 = 1$	(0, 0)	1	Center-node
$\alpha_1 = -1, \alpha_2 = -1, \alpha_3 = 1$	(0, 0)	1	Center-node
$\alpha_1 = 1, \alpha_2 = 1, \alpha_3 = -1$	(0, 0)	-3.63	Saddle-node
$\alpha_1 = 1, \alpha_2 = -1, \alpha_3 = -1$	(0, 0)	-1	Saddle-node

Table 4. Equilibrium Point Classifications of the System (10) Under Different Parameter Choices for α_1, α_2, and α_3

$$\left(\frac{\alpha_2 + \sqrt{\alpha_2^2 + 4\alpha_1\alpha_3}}{2\alpha_1}, 0\right) \quad \text{and} \quad \left(\frac{\alpha_2 - \sqrt{\alpha_2^2 + 4\alpha_1\alpha_3}}{2\alpha_1}, 0\right)$$

These points represent different dynamical behaviors. Additionally, periodic orbits are observed around the center, and a homoclinic orbit exists at the origin.

Result 2: When $\alpha_1 < 0$, $\alpha_3 < 0$, and $\alpha_2^2 + 4\alpha_1\alpha_3 > 0$, the system has one saddle point at $(0, 0)$ and two centers located at:

$$\left(\frac{\alpha_2 + \sqrt{\alpha_2^2 + 4\alpha_1\alpha_3}}{2\alpha_1}, 0\right) \quad \text{and} \quad \left(\frac{\alpha_2 - \sqrt{\alpha_2^2 + 4\alpha_1\alpha_3}}{2\alpha_1}, 0\right)$$

This configuration results in a homoclinic orbit around the origin, as well as a family of periodic orbits. These structures point to the presence of periodic, solitary, and breaking wave solutions in the system's dynamics.

Result 3: For $\alpha_2^2 + 4\alpha_1\alpha_3 > 0$ and $\alpha_1\alpha_3 < 0$, the system has a center point at:

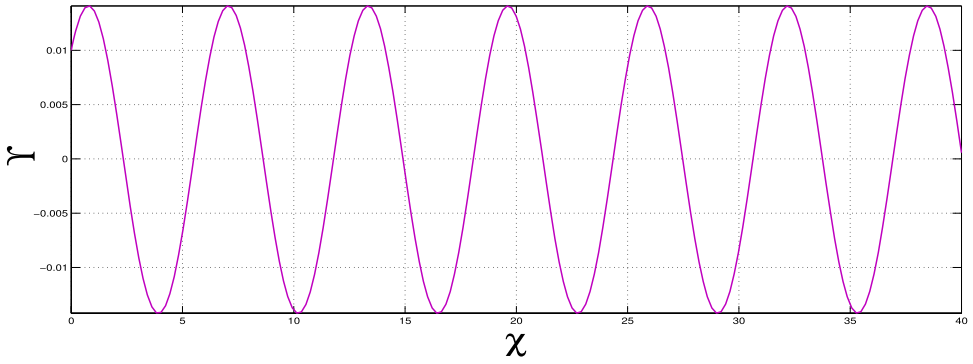

Fig. 9. Nonlinear periodic wave solutions of dynamical system (10) for $\alpha_1, \alpha_2, \alpha_3 > 0$.

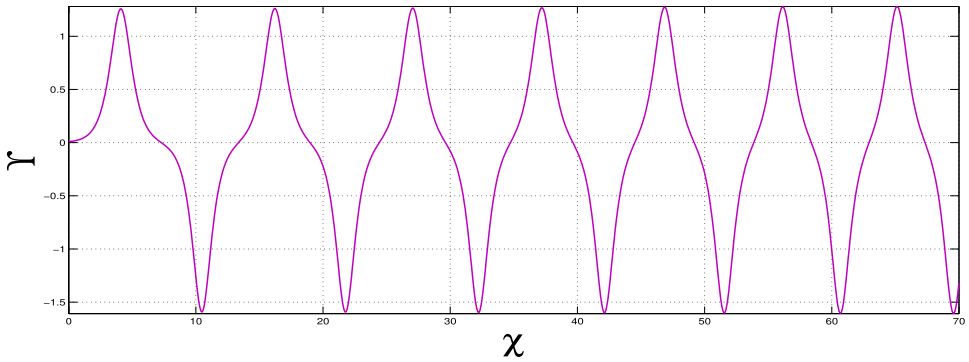

Fig. 10. Supernonlinear periodic wave solutions of dynamical system (10) for $\alpha_1 = -1$, $\alpha_2 = -1$ and $\alpha_3 = 1$.

$$\left(\frac{\alpha_2 - \sqrt{\alpha_2^2 + 4\alpha_1\alpha_3}}{2\alpha_1}, 0\right)$$

This center point is accompanied by two saddle points, one at the origin and another at

$$\left(\frac{\alpha_2 + \sqrt{\alpha_2^2 + 4\alpha_1\alpha_3}}{2\alpha_1}, 0\right)$$

This configuration leads to a series of periodic orbits near the center, alongside a homoclinic orbit at the origin. The system exhibits a variety of periodic, solitary, and breaking wave solutions.

Result 4: When $\alpha_2^2 + 4\alpha_1\alpha_3 < 0$, the system has a single equilibrium point at (0,0). This point is saddle if $\alpha_3 < 0$, and a center if $\alpha_3 > 0$. The system also shows a series of bounded open orbits, supporting periodic and breaking wave solutions.

Result 5: When $\alpha_2^2 + 4\alpha_1\alpha_3 = 0$, the system defined by equation (10) has one center point at $(0, 0)$ and one saddle point at

$$\left(\frac{\alpha_2}{2\alpha_1}, 0\right).$$

Wave solutions of the dynamical system

To find all possible super-nonlinear wave solutions, we need to figure out all the super-nonlinear paths for system (10) by changing the physical parameters α_1, α_2, and α_3. By systematically adjusting parameters, we illustrate both periodic and super-periodic wave solutions. These results, shown in Figs. 9 and 10, clearly demonstrate that the system can support different types of nonlinear wave behaviors.

Our results clearly show that there are nonlinear periodic wave solutions, as seen in Fig. 9, which shows waves that repeat over time due to nonlinear effects in the system. Additionally, super-nonlinear periodic wave solutions, shown in Fig. 10, are a more complicated type of solution that features stronger nonlinear interactions and more complex wave shapes than regular nonlinear periodic waves. These findings point out the many

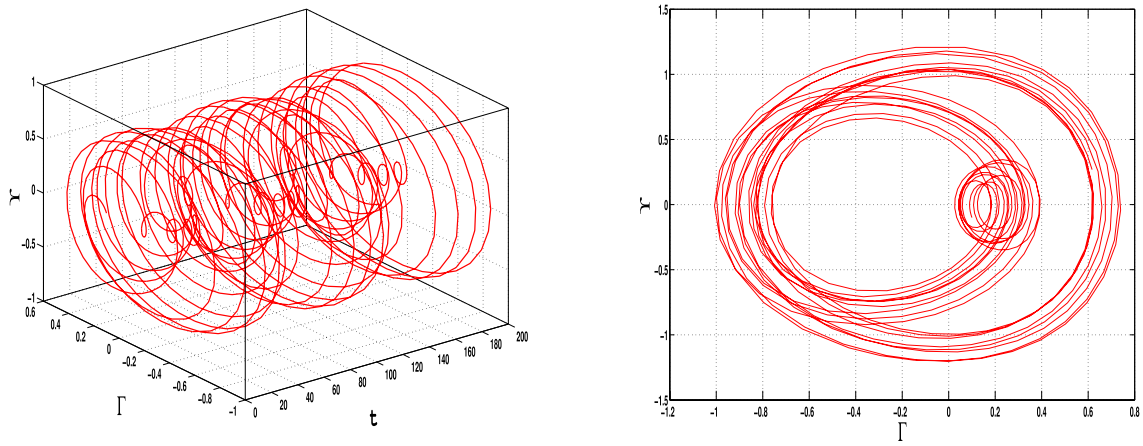

(a) 3D Quasiperiodic Dynamics (b) 2D Quasiperiodic Dynamics

Fig. 11. The 3D and 2D phase portraits of the system (11) for $\alpha_1 = -1, \alpha_2 = 1, \alpha_3 = 1A_0 = 0.6$ and $\tau = 1.6$.

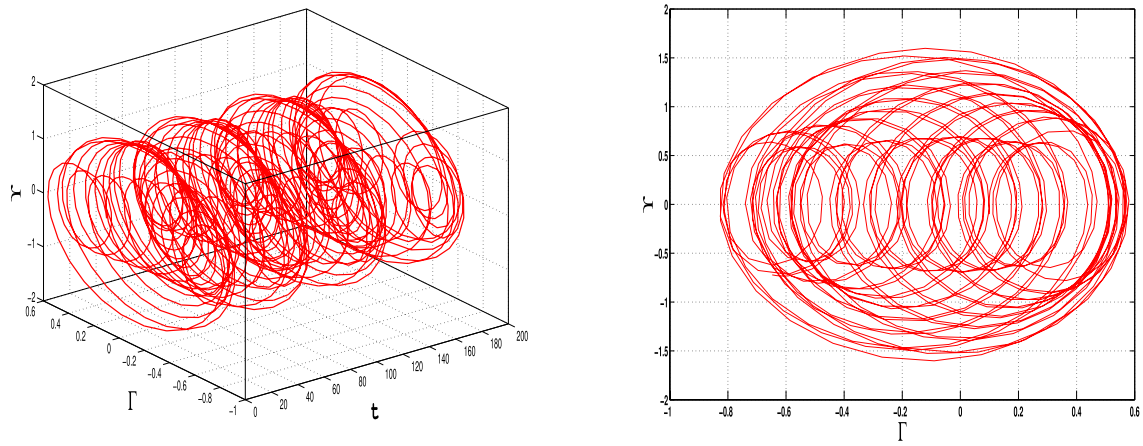

(a) 3D Quasi-Periodic Dynamics (b) 2D Quasi-Periodic Dynamics

Fig. 12. The 3D and 2D phase portraits of the system (11) for for $\alpha_1 = -1, \alpha_2 = 1, \alpha_3 = 1A_0 = 2.5$ and $\tau = 3$.

aspects and levels of detail within the system under study, giving profound insight into the formation of super-nonlinear waves.

Analysis of quasi-periodic behaviour

In this section, we study the quasiperiodic patterns of the considered model. We explore the quasi-periodic dynamics of the system under three distinct parameter sets, visualizing the results using 2D and 3D phase portraits alongside corresponding time series plots. These visualizations provide a complete view of how the system's behavior is controlled by parameter change, with subtle interactions between more than one frequency and their impact on stability and predictability.

The perturbed form of Eq (10) after inserting the periodic term $A_0 \cos(\tau t)$ is:

$$\Upsilon' = \Gamma, \quad \Gamma' = \alpha_1 \Upsilon^3 - \alpha_2 \Upsilon^2 - \alpha_3 \Upsilon + A_0 \cos(\tau t), \tag{11}$$

where A_0 is the amplitude and τ is the frequency of the external forcing.

The results shown in Figs. 11, 12, and 13 for each set of parameters have the defining characteristics of quasi-periodic behavior: bounded but non-repeating orbits for the 2D and 3D plots. This analysis highlights the system's sensitivity to parameter changes and captures the intricate, deterministic patterns that govern its behavior. These results are necessary to advance our understanding of nonlinear dynamical systems and their

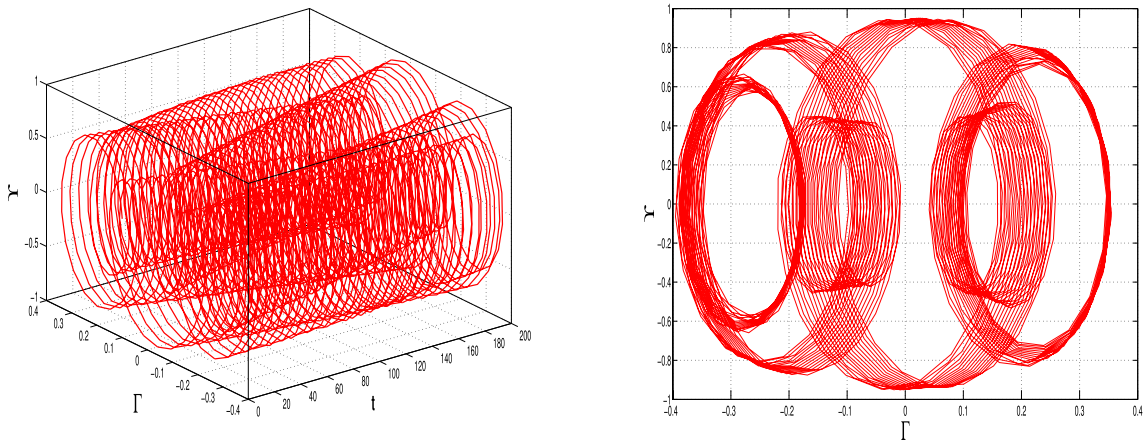

(a) 3D Quasi-Periodic Dynamics (b) 2D Quasi-Periodic Dynamics

Fig. 13. The 3D and 2D phase portraits of the system (11) for for $\alpha_1 = -1, \alpha_2 = 1, \alpha_3 = 1 A_0 = 4$ and $\tau = 6$.

Time	Lyapunov Exp1	Lyapunov Exp2
0.1000	0.1008	−0.1008
0.2000	0.9533	−0.9533
0.5000	0.2450	−0.2460
10.0000	0.1235	−0.1235
15.0000	0.3231	−0.3231
20.0000	0.1815	−0.1815
30.0000	0.1625	−0.1625
40.0000	0.1420	−0.1420
50.0000	0.1549	−0.1548
60.0000	0.1156	−0.1156
80.0000	0.1140	−0.1140
100.0000	0.1028	−0.1028

Table 5. Temporal Variation of Lyapunov Exponents.

potential for applications in real systems. The quasi-periodic patterns that were noted highlight the intricate dynamics of the system, opening the way for a detailed study of chaos through Lyapunov exponent analysis.

Quantitative insights into dynamical system behavior using Lyapunov exponents

Lyapunov exponents are the fundamental quantities that characterize the stability and chaos of dynamical systems. A positive Lyapunov exponent signals exponential divergence of close trajectories, suggesting chaos, while a negative one suggests convergence to a stable state. The results in Table 5 show how the Lyapunov exponents change over time for the system being studied, and Fig. 14 also supports its chaotic behavior with the highest positive Lyapunov exponent of 0.9533. This indication highlights the sensitivity of the system to changes in parameters and initial conditions, giving quantitative verification of the occurrence of chaos. These findings are significant in comprehending the inherent dynamics of nonlinear systems and their potential applications in optimization and control.

Poincaré analysis for detecting quasi-periodic and chaotic behaviors

The Poincaré map is a powerful mathematical and visualization technique for analyzing nonlinear dynamical systems. We demonstrate its usefulness in this paper by its capability to distinguish between quasi-periodic and chaotic behavior. Figure 15-a shows a quasi-periodic motion with $\alpha_1 = -1, \alpha_2 = 1, \alpha_3 = 1, A_0 = 0.09$, and $\tau = 1.2$, where the points form a closed and repeating pattern in the Poincaré map. This pattern indicates regularity and stability in the system. In contrast, Fig. 15-b shows chaotic movement when $\alpha_1 = -1, \alpha_2 = 1, \alpha_3 = 1, A_0 = 0.8$, and $\tau = 1.2$, where the scattered points show randomness and how small changes at the start can lead to different outcomes. The results highlight the role of Poincaré maps in identifying complex system behavior and transitions. The results demonstrate how the system reacts to changes in parameters and confirm

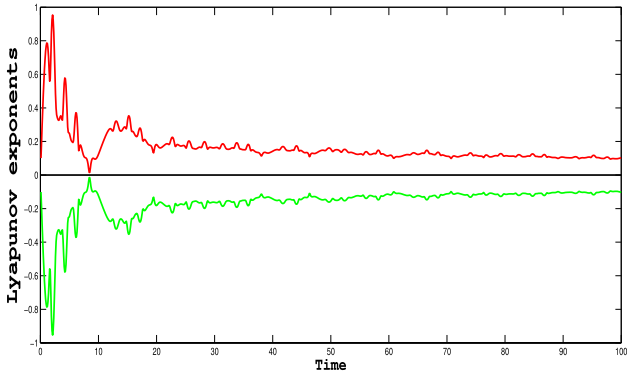

Fig. 14. Dynamics of the Lyapunov exponent for the model (11) for the parameters values of $\alpha_1 = -1, \alpha_2 = -1, \alpha_3 = -1$, $A_0 = 0.2$ and $\tau = 0.86$.

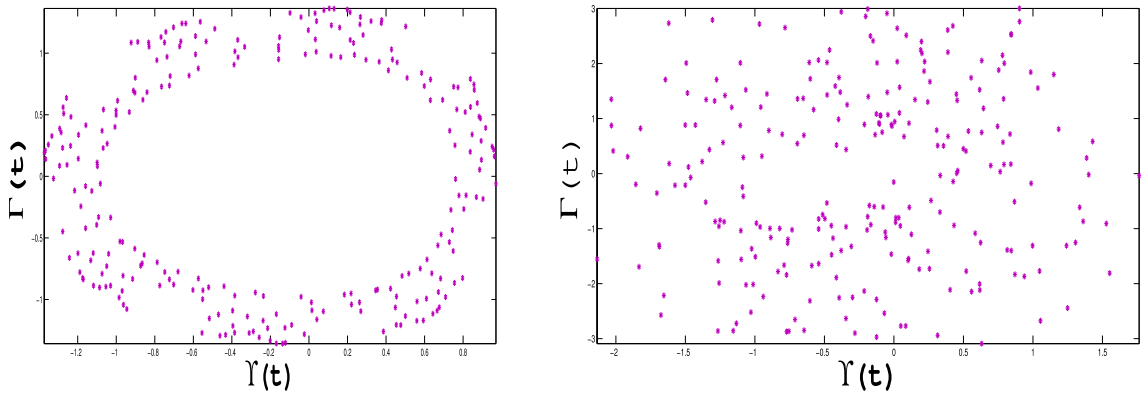

(a) Quasi periodic motion (b) Chaotic motion

Fig. 15. Poincaré maps for the dynamical system (11).

that this technique is helpful for studying nonlinear dynamics, such as in improving and managing industrial processes.

Sensitivity analysis

Sensitivity analysis is the powerful technique that enables one to examine how changes in the input or model parameters alter the output of a system; this provides critical insights into its behavior[33,34]. The results depicted in Figs. 16, 17 and 18) clearly illustrate the system's sensitivity to initial conditions, confirming the presence of chaotic behavior. These graphs highlight the fundamental aspect of chaos—extreme sensitivity to initial conditions—observed for specific parameter values.

Using the initial conditions outlined in Table 6, we systematically examine how perturbations influence the behavior of the perturbed dynamical system ((11)). The findings underscore the intricate interplay between system parameters and initial states, demonstrating the critical role of sensitivity analysis in uncovering the rich dynamics of chaotic systems[28].

Interpretation of results and applications

The results from this research have greatly contributed to increasing knowledge on Gardner-KP type equations. Most previous studies have dealt with (2+1)-dimensional Gardner-KP and related equations[20–22,25,26], mainly investigating simple soliton patterns such as single solitons, lumps and breathers. On the other hand, this study on the (3+1)-dimensional Gardner-KP equation reveals various soliton profiles, like double periodic waves, shock waves and kink-type solitons.

A thorough study of the system here discovers new kinds of stability and leads to chaotic behavior that past studies have rarely described. It is evident from this that (3+1)-dimensional models are better for reflecting the various aspects of nonlinear waves in physical systems.

Multiple fields could make use of the outcomes from this work.

- Ocean Engineering plays a role by studying how internal waves travel along the ocean's shelves and impact movement of sediments and shaping of coasts.

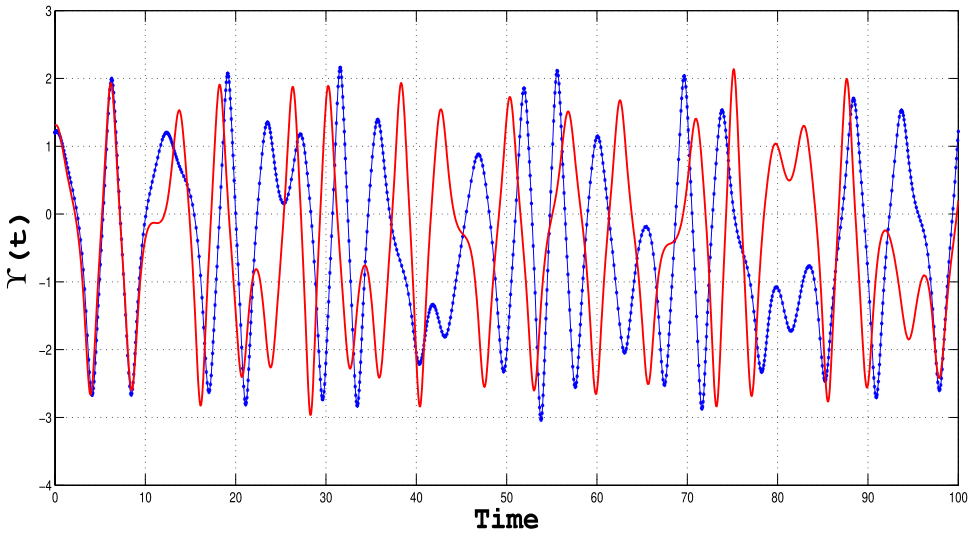

Fig. 16. Sensitivity plot for the perturbed dynamical system given in equation ((11)), using the specified parameters and initial conditions outlined in the table.

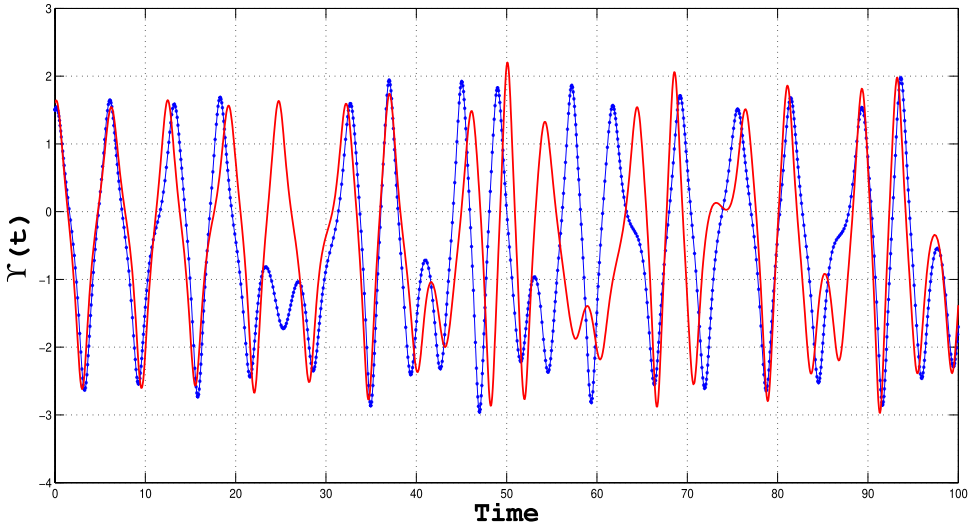

Fig. 17. Sensitivity plot for the perturbed dynamical system given in equation ((11)), using the specified parameters and initial conditions outlined in the table.

- Exploring wave distributions in plasma which cover solitary pulses and shock waves important for energy processes.
- how solitons behave in optical fibers, necessary for securing the digital signal of communication systems.
- Bose-Einstein Condensates with their self-organizing nature help us study nonlinear waves and their stability in quantum fluids.

Overall, this study broadens the application of Gardner-KP models in several scientific fields by adding concepts and explanations for practical use.

Conclusion

We investigated the non-linear $(3+1)$-dimensional KP-Gardner equation, focusing on its soliton solutions and dynamical behaviors. Using the Jacobi elliptic method, we derived soliton solutions that illustrate the equation's rich nonlinear wave dynamics. These solitons provide valuable insights into wave transmission dynamics, with applications in various fields of physics and engineering. We conducted the dynamical analysis using the phase plane analysis, which provided a detailed classification of phase portraits based on orbital structures. Sensitivity analysis results were presented to highlight the system's dependence on parameter variations. We used the Runge-Kutta (RK) method to solve the model, which indicated the existence of both supernonlinear and nonlinear periodic wave patterns. We further explored the effects of physical constants on quasi-periodic and

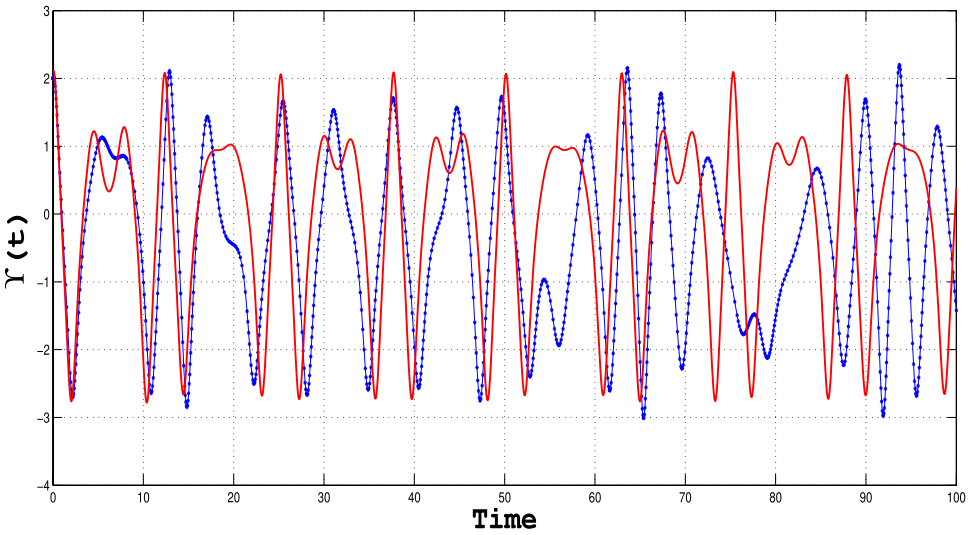

Fig. 18. Sensitivity plot for the perturbed dynamical system given in equation ((11)), using the specified parameters and initial conditions outlined in the table.

	Initial conditions data		
Dynamical system Type	Figure	Blue Curve	Red Curve
System ((11))	16	(1.2,0.2)	(1.3, 0.3)
System ((11))	17	(1.5,0.5)	(1.6,0.6)
System ((11))	18	(2,0.6)	(2.1,0.6)

Table 6. Parametric values for sensitivity analysis.

chaotic patterns within the perturbed dynamical system. To confirm chaotic behavior, Lyapunov exponents were calculated, Poincaré sections were plotted, and sensitivity analysis was performed. Changes in the frequencies and strengths of outside disturbances greatly affect the system's unpredictable, chaotic behavior, as these analyses revealed. The results have profound implications for applications in engineering, fiber optics, and other scientific disciplines, where nonlinear models are critical to advancing theoretical and practical innovations.

Data availability

The datasets used and/or analysed during the current study available from the corresponding author on reasonable request.

Received: 28 April 2025; Accepted: 3 October 2025
Published online: 23 October 2025

References

1. Miah, M. M., Alsharif, F., Iqbal, M. A., Borhan, J. R. M. & Kanan, M. Chaotic Phenomena Sensitivity Analysis, Bifurcation Analysis, and New Abundant Solitary Wave Structures of Two Nonlinear Dynamical Models in Industrial Optimization. *Mathematics* **12**, 1959 (2024).
2. Guckenheimer, J. & Holmes, P. *Nonlinear Oscillations, Dynamical Systems, and Bifurcations of Vector Fields* (Springer-Verlag, New York, 1983).
3. Kuznetsov, Y. A. *Elements of Applied Bifurcation Theory* 3rd edn. (Springer-Verlag, New York, 2004).
4. Lenells, J. Stability for the periodic Camassa-Holm equation. *Math. Scand.* **97**, 188–200 (2005).
5. Bödeker, H. U., Röttger, M. C., Liehr, A. W., Frank, T. D. & Friedrich, R. Noise-covered drift bifurcation of dissipative solitons in a planar gas-discharge system. *Phys. Rev. E* **67**, 046218 (2003).
6. Ullah, M. S., Ali, M. Z. & Roshid, H. O. Bifurcation analysis and new waveforms to the first fractional WBBM equation. *Sci. Rep.* **14**, 11907 (2024).
7. Rizvi, S. T., Abdelkawy, M. A., Zahed, H. & Seadawy, A. R. Advanced study of nonlinear partial differential equations in ion-acoustic and light pulses: solitons, chaos, and energy perspectives. *AIMS Mathematics* **10**(5), 11842–11879 (2025).
8. Alam, N., Ma, W.-X., Ullah, M. S., Seadawy, A. R. & Akter, M. Exploration of soliton structures in the Hirota-Maccari system with stability analysis. *Mod. Phys. Lett. B* **39**(11), 2450481 (2025).
9. Chen, Y., & Li, S. New traveling wave solutions and interesting bifurcation phenomena of generalized KdV-MKdV-like equation *Adv. Math. Phys.* 103049, (2021).
10. Gordon, J. P. & Haus, H. A. Solitons in optical fibers. *IEEE J. Quantum Electron.* **22**, 873–879 (1986).
11. Abbas, N. & Hussain, A. Novel soliton structures and dynamical behaviour of coupled Higgs field equations. *Eur. Phys. J. Plus* **139**, 1–14 (2024).

12. Hussain, A., Abbas, N., Niazai, S. & Khan, I. Dynamical behavior of the Lakshmanan-Porsezian-Daniel model with spatiotemporal dispersion effects. *Alexandria Eng. J.* **96**, 332–343 (2024).
13. Hussain, A. & Abbas, N. Periodic, quasi-periodic, chaotic waves and solitonic structures of coupled Benjamin-Bona-Mahony-KDV system. *Physica Scripta* **99**, 125231 (2024).
14. Dipankar, K. Bifurcations of phase portraits and chaotic behaviors of the (2+1)-dimensional double-chain DNA system with beta derivative: A qualitative approach. *Heliyon* **10**, 14 (2024).
15. Ruderman, M. S., Talipova, T. & Pelinovsky, E. Dynamics of modulationally unstable ion-acoustic wavepackets in plasmas with negative ions. *J. Plasma Phys.* **74**, 639–656 (2008).
16. Kamchatnov, A. M., Kartashov, Y. V., Larre, P.-E. & Pavloff, N. Nonlinear polarization waves in a two-component Bose-Einstein condensate. *Phys. Rev. A.* **89**, 033618 (2014).
17. Ganie, A. H. et al. Bifurcation, chaos, and soliton analysis of the Manakov equation. *Nonlinear Dyn.* **113**, 9807–9821 (2025).
18. Ullah, M. S., Ali, M. Z. & Roshid, H. O. Stability analysis, ϕ^6 model expansion method, and diverse chaos-detecting tools for the DSKP model. *Sci. Rep.* **15**, 13658 (2025).
19. Rahaman, M. S., Islam, M. N. & Ullah, M. S. Bifurcation, chaos, modulation instability, and soliton analysis of the Schrödinger equation with cubic nonlinearity. *Sci. Rep.* **15**, 11689 (2025).
20. Chen, P. L. F. & Liu,. A generalized modified Kadomtsev-Petviashvili equation for interfacial wave propagation near the critical depth level. *Wave Motion* **27**(3), 321–339 (1988).
21. Aslanova, G., Ahmetolan, S. & Demirci, A. Nonlinear modulation of periodic waves in the cylindrical Gardner equation. *Phys. Rev. E* **102**, 052215 (2020).
22. Tariq, K. U., Seadawy, A. R. & Alamri, S. Z. Computational soliton solutions to (3+1)-dimensional generalised Kadomtsev-Petviashvili and (2+1)-dimensional Gardner-Kadomtsev-Petviashvili models and their applications. *Pramana J. Phys.* **91**(68), 1–13 (2018).
23. Boateng, K., Yang, W., Yaro, D. & Otoo, M. E. Jacobi elliptic function solutions and traveling wave solutions of the (2+ 1)-dimensional Gardner-KP equation. *Math. Methods Appl. Sci.* **43**, 3457–3472 (2020).
24. Wazwaz, A. M. Solitons and singular solitons for the Gardner-KP equation. *Appl. Math. Comput.* **204**, 162–169 (2008).
25. Aslanova, G., Demirci, A. & Ahmetolan, S. Modulated periodic wavetrains in the spherical Gardner equation. *Wave Motion* **109**, 102844 (2022).
26. Hussain, A. et al. Symmetries, optimal system, exact and soliton solutions of (3 + 1)-dimensional Gardner-KP equation. *J. Ocean Eng. Sci.* **9**, 178–190 (2024).
27. Elboree, M. K. The Jacobi elliptic function method and its application for two component BKP hierarchy equations. *Computers & Mathematics with Applications* **62**(12), 4402–4414 (2011).
28. Strogatz, S. H. *Nonlinear Dynamics and Chaos: with Applications to Physics, Biology, Chemistry, and Engineering* 2nd edn. (Westview Press, Boulder, CO, 2015).
29. Jacobi, C. G. J. New foundations of the theory of elliptic functions, Königsberg, (1829).
30. Drazin, P. G. & Johnson, R. S. *Solitons: An Introduction* (Cambridge University Press, 1989).
31. Kapitula, T. & Promislow, K. *Spectral and Dynamical Stability of Nonlinear Waves* (Springer, 2013).
32. Goldstein, H., Poole, C., & Safko, J. Classical Mechanics, 3rd ed., Pearson, (2002).
33. Saltelli, A., Tarantola, S., Campolongo, F. & Ratto, M. **Sensitivity Analysis in Practice: A Guide to Assessing Scientific Models** (Wiley, 2004).
34. Ali, A., Ahmad, J. & Javed, S. Exploring the Dynamic Nature of Soliton Solutions to the Fractional Coupled Nonlinear Schrödinger Model With Their Sensitivity Analysis. *Optical and Quantum Electronics* **55**(9), 810 (2023).

Acknowledgements

This article has been produced with the financial support of the European Union under the REFRESH – Research Excellence For Region Sustainability and High-tech Industries project number CZ .10.03.01/00/22_003/0000048 via the Operational Programme Just Transition.

Author contributions

Amjad Hussain: Conceptualization, Methodology, Writing- Reviewing and Editing, Supervision. Muhammad Zeeshan: Data curation, Writing- Original draft preparation. M.J. Rehman: Visualization, Investigation. Adil Jhangeer: Visualization, Validation, Methodology, Project administration, Funding Acquisition, Reviewing and editing draft.

Declarations

Competing interests

The authors declare no competing interests.

Additional information

Correspondence and requests for materials should be addressed to A.H.

Reprints and permissions information is available at www.nature.com/reprints.

Publisher's note Springer Nature remains neutral with regard to jurisdictional claims in published maps and institutional affiliations.